Composites Part B 183 (2020) 107600

Contents lists available at ScienceDirect

Composites Part B

journal homepage: www.elsevier.com/locate/composites

Electrical conductivity of CNT/polymer composites: 3D printing, measurements and modeling

A. Mora, P. Verma, S. Kumar *

Department of Mechanical Engineering, Khalifa University of Science and Technology, Masdar City Campus, PO Box 54224, Abu Dhabi, United Arab Emirates

ARTICLE INFO

Keywords:
Carbon nanotubes
Segregation
Agglomeration
Polymer nanocomposites
Additive manufacturing

ABSTRACT

We present electrical conductivity measurements and modeling aspects of carbon nanotube (CNT)/polymer composites enabled via fused filament fabrication (FFF) additive manufacturing (AM). CNT/polylactic acid (PLA) and CNT/high density polyethylene (HDPE) filament feedstocks were synthesized through melt blending with controlled CNT loading to realize 3D printed polymer nanocomposites. Electrical conductivity of 3D printed CNT/PLA and CNT/HDPE composites was measured for various CNT loadings. Low percolation thresholds were obtained from measured data as 0.23 vol. % and 0.18 vol. % of CNTs for CNT/PLA and CNT/HDPE nanocomposites, respectively. Moreover, a micromechanics-based two-parameter agglomeration model was developed to predict the electrical conductivity of CNT/polymer composites. We further show that the two agglomeration parameters can also be used to describe segregated structures, wherein nanofillers are constrained to certain locations within the matrix. To the best of our knowledge, this is the first ever electrical conductivity model to account for segregation of CNTs in the matrix. A good agreement between measured conductivity and predictions demonstrates the adequacy of the proposed model. We further evince the robustness of the model by accurately capturing the conductivity measurements reported in the literature for both elastomeric and thermoplastic nanocomposites. The findings of the study would provide guidelines for the design of electro-conductive polymer nanocomposites.

1. Introduction

Multifunctional materials have been obtained by the addition of nanoparticles into a pristine polymer matrix. Since their popularization by Iijima [1], carbon nanotubes (CNTs) have been widely used to develop multifunctional polymer composites due to their exceptional electrical, thermal and mechanical properties [2–4]. Electro-conductive polymer nanocomposites (PNCs) have been widely used for applications such as interference shielding [5,6], anti-static performance [7], flexible electronics [8,9], damage identification [10], and strain sensing [11,12].

Electrical conduction in PNCs is achieved via inter-aggregate conduction, field emission and tunneling of electrons [13]. The conduction mechanism can be defined on the basis of filler distribution namely their separation (above or below the tunneling cutoff) or contact (conducting network) [13,14]. Electrical conduction is possible either due to inter-particle contact or electrons being able to jump from one CNT to the other through a thin polymer layer (tunneling effect). In this way, CNTs form a continuous conductive network, i.e., a percolated network. The formation of a percolated network is possible above a critical CNT concentration, i.e., the percolation threshold [14]. Electrons move from one end to the other of a percolated network under an applied electrical field, leading to an increase in the electrical conductivity of several orders of magnitude. Since CNTs need to be close to each other to be part of the percolated network, dispersion quality is an important parameter. In contrast, agglomeration of CNTs makes it more difficult for CNTs to form a network that spans the entire domain of the nanocomposite [2]. However, a non-homogeneous distribution of CNTs can actually result in higher electrical conductivity at lower loadings by the CNTs forming a segregated structure [15]. In a segregated structure, nanofillers are constrained at certain locations inside the polymer matrix. This results in regions where, locally, there is a higher concentration of CNTs compared to the overall content inside the polymer. Then, the percolation threshold is reduced as the CNTs are closer to each other in these regions of high CNT concentration, attributing to the formation of a conductive nanocomposite at lower CNT loading [15,16].

There are several ways to fabricate electrically conductive PNCs such as melt blending, solvent casting, and in-situ polymerization [17]. Recently additive manufacturing, also known as three-dimensional printing (3DP), has been widely adopted for the fabrication of PNCs.

* Corresponding author.
E-mail address: s.kumar@eng.oxon.org (S. Kumar).

https://doi.org/10.1016/j.compositesb.2019.107600
Received 5 September 2019; Received in revised form 30 October 2019; Accepted 12 November 2019
Available online 19 November 2019

3DP is rapidly advancing towards new materials and applications owing to its technological flexibility and unique features compared to conventional manufacturing techniques [18–20]. Among all 3DP technologies, fused filament fabrication (FFF) is attaining more appreciation because of low processing and machinery cost, operational simplicity with high reliability, material selection flexibility, among others [21–25]. Furthermore, as the interest for developing PNCs with multifunctional attributes is gaining industrial importance, computational models that aid in their design are also becoming important.

Different computational models have been developed for predicting and analyzing the electro-conductive characteristics of CNT-based PNCs [26–28]. Many models reported thus far assumed homogeneous distribution of CNTs within the matrix [26,28–31]. A few other studies considered the effects of CNT agglomeration [32,33]. Nevertheless, these agglomeration models cannot capture the electrical conductivity of PNCs that exhibit segregated filler dispersions. Our 3D printed PNCs show segregated dispersion of CNTs. Therefore, an electrical conductivity model for PNCs that captures the segregation of CNT is indispensable. This, further justifies the need for of an electrical conductivity model for PNCs which accounts for segregation and agglomeration. Indeed, the closest models to consider segregation are the works of Mora et al. [34] and Park et al. [35]. On one hand, Mora et al. [34] presented a computational model for the electrical conductivity of polymers loaded with hybrid particles that consist of CNTs grown on graphene nanoplatelets [36]. Although, the network of hybrid particles forms a segregated structure, the hybrid particles themselves are homogeneously distributed. On the other hand, Park et al. [35] presented a computational model for CNT/silica/polymer composites. In their work, it was the addition of micron-sized silica particles that caused segregation of CNTs. Other approaches to model electrical conductivity of segregated structures in CNT-based PNCs have not been reported.

Thus, in this work we prepared CNT/polylactic acid (PLA) and CNT/high-density polyethylene (HDPE) PNCs via FFF with varying CNT contents utilizing in-house nano-engineered filament feedstocks. The morphology of the fabricated PNCs was studied via scanning electron microscopy (SEM) and electrical conductivities at different CNTs contents were measured. A micromechanics-based electrical conductivity model was developed to study the PNCs herein fabricated. We used a two-parameter agglomeration model and showed that it can also be used for segregated structures. Measurements obtained for CNT/PLA and CNT/HDPE nanocomposites as well as for other nanocomposites reported in the literature were reproduced with our agglomeration and segregation model. The rest of the article is organized as follows. In Section 2 we present the experimental details for the preparation and measurement of electrical conductivity of CNT/PLA and CNT/HDPE nanocomposites. Then, in Section 3 we describe the electrical conductivity model for agglomeration and segregation. In Section 4 we present our results on CNT characterization, electrical conductivity measurements and results from our model for agglomeration and segregation. Finally, we present our conclusions in the last section.

2. Materials and experimental methods

2.1. Materials

PLA grade Inge^{TM} 3D850 developed by NatureWorks having a melt flow index of 9 g/10 min (230 °C/2.16 kg) and HDPE with a melt flow index of 1.3 g/10 min (190 °C/5 kg) supplied by Borouge Pte Ltd, were used as polymer matrices for the fabrication of filament feedstocks. From differential scanning calorimetry (DSC) analysis (see Figure SI.1), the melting and glass transition temperatures of PLA were observed to be 172 °C and 70 °C, respectively, while the melting and crystalline temperatures of HDPE were observed to be 134 °C and 109 °C, respectively. DSC results also confirmed the amorphous nature of PLA and semi-crystalline nature of HDPE with crystallinity ~ 45 %. Multi-walled carbon nanotubes (referred to simply as CNTs in the rest of the article) were supplied by Applied Nanostructured Solution, LLC.

2.2. Development of CNT/PLA and CNT/HDPE nanocomposite filaments for FFF 3D printing

CNT/PLA and CNT/HDPE nanocomposite filaments were prepared via melt mixing process using co-rotating Coperion ZSK 18 (Germany) twin-screw extruder (TSE) having a screw of diameter D = 18 mm and L/D = 40, where L is the screw length. The temperature in the 1st, 3rd, 5th, 7th, 9th zone and die was kept as 160, 180, 190, 210, and 220 °C, respectively with a screw speed of 200 rpm. Here, the 1st and 2nd zones correspond to the feed zone of the 3D printer; the 3rd, 4th, 5th and 6th zones correspond to the melting zone; and the 7th, 8th and 9th zones correspond to the melt processing zone. Before compounding, polymer (PLA and HDPE) and CNTs were vacuum dried at 60 °C and 100 °C respectively for 24 h. Subsequently, PLA/CNT and HDPE/CNT were mixed manually with the help of a solvent (acetone) for better mixing before being fed into the extruder. The CNT/polymer composites were extruded using a circular die of 1.80 mm diameter and, to maintain a consistency of filament diameter (of 1.74 mm), speed roller was used. CNT/PLA composites were prepared by mixing varying amounts of CNT content and designated as PLA-0, PLA-0.25, PLA-0.5, PLA-1, PLA-2 and PLA-4. Likewise, CNT/HDPE composites were designated as HDPE-0, HDPE-0.25, HDPE-0.5, HDPE-1, HDPE-2, HDPE-4 and HDPE-6. Here, the numeric term (i.e., 0, 0.25, 0.5, 1, 2, 4 and 6) stands for actual loading level of CNT in percentage of weight fraction.

2.3. Additive manufacturing of nanocomposites using FFF technique

3D printing of samples utilizing in-house developed filaments was carried out using Creator Pro Flash Forge 3D printer and Simplify3D slicing software. CAD files were prepared using Solidworks and transferred to a 3D compatible STL file. The laboratory-made filament was fed into a 0.4 mm diameter nozzle by a feeding pressure mechanism via a driver motor and a counter-rotating set of grooved gears. Process parameters such as nozzle tip temperature (220 °C for PLA and 250 °C for HDPE), bed temperature (65 °C for PLA and 120 °C for HDPE), layer height (0.2 mm), infill density (100%), extrusion width (0.4 mm), nozzle movement speed (2700 mm/min for PLA and 900 mm/min for HDPE), first layer (300 mm/min), layer height (0.18 mm), extrusion width (0.48 mm), infill pattern (rectilinear) were kept constant for all the specimens.

2.4. Characterization

Scanning electron microscopy (Nova Nano SEM 50 series, operated at 10 kV) technique was used to examine the surface morphology and dispersion state of CNTs in the polymer matrix. Raman spectroscopy (Witech Alpha 300RAS Raman spectrometer with wave length 532 nm) and X-ray diffraction (PANalytical instrument X'pert PRO Netherlands, using Ni filtered Cu-Kα radiation) were used to evaluate the structure of CNTs. The purity of CNTs was quantified using thermogravimetric analysis (TGA) in oxygen atmosphere (flow rate 10 ml/min) using TA instrument Q-50. The DC electrical conductivity of the CNT/polymer nanocomposite samples was measured using four probe van der Pauw method. For this test, square samples of size 10 mm × 10 mm with 2 mm thickness were fabricated by 3D printing. Silver paste was applied on the four corners of the samples to facilitate electrical contact between the electrodes and the sample.

3. Electrical conductivity model for agglomeration and segregation of cnts

In this section we first present a micromechanics-based model for predicting electrical conductivity of CNTs homogeneously distributed into a matrix. Then, we introduce the two-parameter model for agglomeration. We present a new perspective on the two agglomeration parameters and show that they can be used to represent segregation.

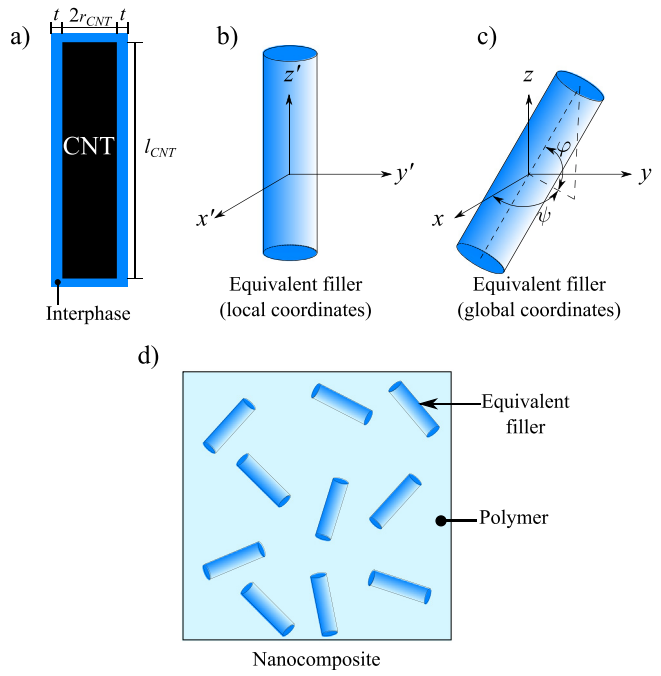

Fig. 1. (a) A CNT and its surrounding interphase, (b) equivalent filler shown in local coordinates, (c) equivalent filler shown in global coordinates, and (d) equivalent fillers that are randomly distributed in a polymer matrix.

In that way, a wider range of microstructures may be represented using those two parameters. Then, in Section 3.3, we incorporate the two parameters for agglomeration and segregation into the electrical conductivity model.

3.1. Homogeneously dispersed CNTs

Here, CNTs are initially considered to be straight and randomly distributed in a polymer matrix as shown in Fig. 1. Due to tunneling and hopping of electrons, CNTs do not have to be in physical contact in order for electrons to flow from one CNT to the other. Separations in the order of a few nanometers allow for electrons to tunnel from one CNT to the other [37,38]. Thus, to include this behavior in the electrical model, CNTs are considered to be surrounded by an interphase layer of thickness t as illustrated in Fig. 1a. We observe that, for conduction to be possible between two CNTs, their interphases must be overlapping or in contact. As a result, the thickness of the interphase is limited by the cutoff distance for tunneling, d_c, as [30]:

$$t = \frac{1}{2} d_c. \tag{1}$$

The interphase surrounding the CNTs has a conductivity given by [32]:

$$\sigma_{int} = \frac{d_c}{A_T R_J(d_c)}, \tag{2}$$

where A_T is the area for tunneling, and R_J is the junction resistance which is given by [31,39]:

$$R_J = \frac{h^2 d_a}{A_T e^2 \sqrt{2m\lambda}} \exp\left(\frac{4\pi d_a}{h}\sqrt{2m\lambda}\right), \tag{3}$$

where h is Planck's constant ($6.62606957 \times 10^{-34}$ kg m^2/s), d_a is the average separation between CNTs (in the order of a few nm), λ is the height of the barrier (in the order of a few eV), e and m are the charge ($1.602176565 \times 10^{-19}$ C) and mass of an electron ($9.10938291 \times 10^{-31}$ kg), respectively. The average separation between CNTs is approximated by [30]:

$$d_a = \left(\frac{\phi_c}{\phi}\right)^{1/3} d_c, \tag{4}$$

where ϕ and ϕ_c are the CNT volume fraction and percolation threshold, respectively.

The CNT and its surrounding interphase are considered to be an equivalent filler dispersed in the polymer matrix, as shown in the schematic of Fig. 1. The electrical conductivity of this equivalent filler is given by:

$$\sigma_{eq} = \begin{bmatrix} \sigma_{eq}^L & 0 & 0 \\ 0 & \sigma_{eq}^T & 0 \\ 0 & 0 & \sigma_{eq}^T \end{bmatrix}, \tag{5}$$

where σ_{eq}^L and σ_{eq}^T are the longitudinal and transverse electrical conductivities of the equivalent filler. Note that σ_{eq} is given in the local coordinates of the CNT (Fig. 1b). The conductivities of the equivalent filler are calculated from [29,32]:

$$\sigma_{eq}^L = \frac{\left(l_{CNT}+2t\right)\left[r_{CNT}^2\sigma_{CNT}^L + \left(2r_{CNT}t+t^2\right)\sigma_{int}\right]\sigma_{int}}{2r_{CNT}^2 t\sigma_{CNT}^L + 2t\left(2r_{CNT}t+t^2\right)\sigma_{int} + l_{CNT}\left(r_{CNT}+t\right)^2\sigma_{int}}, \tag{6}$$

$$\sigma_{eq}^T = \frac{\sigma_{int}}{l_{CNT}+2t}\left[l_{CNT}\frac{2r_{CNT}^2\sigma_{CNT}^T + \left(\sigma_{CNT}^T+\sigma_{int}\right)\left(2r_{CNT}t+t^2\right)}{2r_{CNT}^2\sigma_{int} + \left(\sigma_{CNT}^T+\sigma_{int}\right)\left(2r_{CNT}t+t^2\right)} + 2t\right], \tag{7}$$

where l_{CNT}, r_{CNT}, σ_{CNT}^L, and σ_{CNT}^T are the CNT length, radius, longitudinal and transverse electrical conductivities, respectively.

Since now the matrix is considered to be loaded with an equivalent filler, its volume fraction needs to be calculated. By considering its volume, the volume fraction of the equivalent filler in the composite is:

$$\phi_{eq} = \frac{\left(r_{CNT}+t\right)^2\left(l_{CNT}+2t\right)}{r_{CNT}^2 l_{CNT}}\phi, \tag{8}$$

where ϕ_{eq} is the volume fraction of the equivalent nanofiller. Since l_{CNT} is typically in the order of microns and t is in the order of a few nanometers, then $l_{CNT} \gg t$ and $l_{CNT} + 2t \approx l_{CNT}$. Thus, in our model we use the approximation:

$$\phi_{eq} = \left(1 + \frac{t}{r_{CNT}}\right)^2 \phi. \tag{9}$$

Following the Mori–Tanaka homogenization scheme [30,32], the electrical conductivity of the equivalent nanofillers is averaged along all possible orientations. In addition, not all CNTs take part of the percolated network. Below the percolation threshold, ϕ_c, electrical conductivity is possible mainly through electron hopping as there is no percolated network. Above ϕ_c, electrical conductivity of the composite is mainly possible through the conductive network. Thus, contributions of both electron hopping and conductive networks are considered. Then, the effective conductivity of the composite is given by:

$$\sigma_{eff} = \sigma_M + (1-\eta)\sigma_{EH} + \eta\sigma_{CN} \tag{10}$$

where σ_M is the conductivity of the matrix, σ_{EH} is the contribution due to electron hopping, σ_{CN} is the contribution due to conductive networks, and η is the fraction of CNTs that participate in the percolated network.

To calculate the fraction of percolated CNTs, we use the simulation results presented by Mora et al. [26], where they present a second degree polynomial to approximate η. However, their approximation has the limitation that η starts decreasing after reaching a maximum value as the CNT content is increased. For simplicity, here we present an exponential function to fit their simulations and approximate η as:

$$\eta = \begin{cases} 0; & 0 \le \phi < \phi_c \\ a\exp\left(b\phi_{red}\right) + 1; & \phi_c \le \phi \le 1, \end{cases} \tag{11}$$

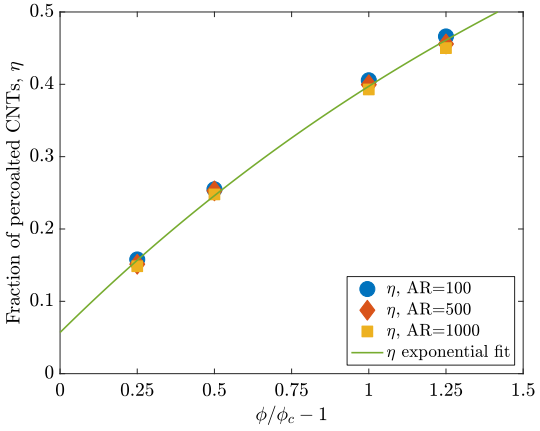

Fig. 2. Approximation of the fraction of percolated CNTs, η, compared with the simulation results obtained by Mora et al. [26] for CNTs with aspect ratio, AR, of 100, 500, and 1000.

where $\phi_{red} = \phi/\phi_c - 1$ is the reduced volume fraction and the fitting parameters are $a = -0.9431$ and $b = -0.4477$. The independent term in Eq. (11) is set to 1 as this is the maximum value that η may have (i.e., when all CNTs participate in the percolated network). In Fig. 2 we compare the exponential fit with the simulation results obtained by Mora et al. [26], where good agreement is obtained. Thus, Eq. (11) is used in our model.

The expressions for σ_{EH} and σ_{CN} in Eq. (10) are given by

$$\sigma_X = \frac{\int_0^{2\pi}\int_0^{\pi} p(\varphi,\psi)\left(Q^T\sigma_{eq}Q - \sigma_M\right)A_X \sin(\varphi)\, d\varphi d\psi}{\int_0^{2\pi}\int_0^{\pi} p(\varphi,\psi)\sin(\varphi)\, d\varphi d\psi} \tag{12}$$

where the subscript X stands for either EH or CN, $p(\varphi,\psi)$ is a distribution function of the CNT orientation with φ and ψ defined as in Fig. 1, Q is a rotation tensor, and A_X is the electric field concentration tensor for electron hopping ($X = EH$) or conductive networks ($X = CN$). For the case of homogeneous distribution of CNTs we have that $p(\varphi,\psi) = 1$. Tensors Q and A_X are given in Eqs. (13) and (14), respectively.

$$Q = \begin{bmatrix} \cos\psi\sin\varphi & \sin\psi\sin\varphi & \cos\varphi \\ -\sin\psi & \cos\psi & 0 \\ -\cos\psi\cos\varphi & -\sin\psi\cos\varphi & \sin\varphi \end{bmatrix} \tag{13}$$

$$A_X = Q^T T_X Q\left[\left(1-\phi_{eq}\right)I + \phi_{eq}\frac{\int_0^{2\pi}\int_0^{\pi} Q^T T_X Q \sin(\varphi)\, d\varphi d\psi}{\int_0^{2\pi}\int_0^{\pi} p(\varphi,\psi)\sin(\varphi)\, d\varphi d\psi}\right]^{-1} \tag{14}$$

In Eq. (14), I is the identity tensor and T_X is given by:

$$T_X = \left[I + S\left(\sigma_M\right)^{-1}\left(\sigma_{eq} - \sigma_M\right)\right]^{-1}, \tag{15}$$

where S is the Eshelby tensor, which has a diagonal form, i.e., $S_{ij} = 0$ for $i \neq j$ and

$$S_{11} = 1 - 2S_{22}, \tag{16}$$

$$S_{22} = S_{33} = \frac{\mu}{2\left(\mu^2-1\right)^{3/2}}\left[\mu\left(\mu^2-1\right)^{1/2} - \cosh^{-1}\mu\right], \tag{17}$$

where μ is the aspect ratio of the CNT. Aspect ratios of CNTs are typically above 100 [40], in which case $\left(\mu^2-1\right)^{1/2} \approx \mu$. We found that when $\mu > 10$, substituting $\left(\mu^2-1\right)^{1/2}$ by μ resulted in a difference below 1%. Thus, using the logarithmic equivalent of $\cosh^{-1}$, we make the following approximation:

$$S_{22} = S_{33}$$

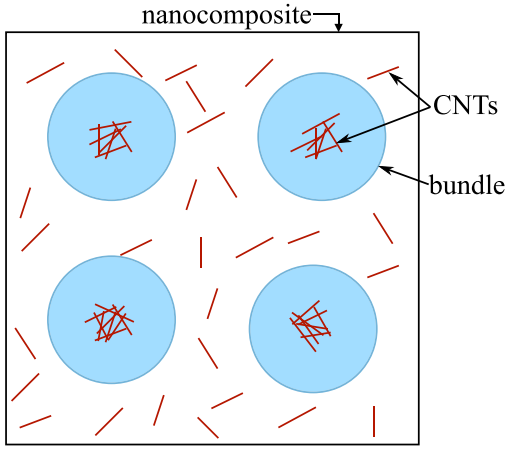

Fig. 3. 2D schematic representation of a CNT/polymer nanocomposite with agglomeration. Blue circles represent bundles (volumes that encapsulate CNT agglomerations) while CNTs are represented as red lines. CNTs are homogeneously distributed outside the bundles in the dispersed matrix (white region).

$$= \begin{cases} \dfrac{\mu}{2\left(\mu^2-1\right)^{3/2}}\left[\mu\left(\mu^2-1\right)^{1/2} - \ln\left(\mu + \left(\mu^2-1\right)^{1/2}\right)\right], & \mu \leq 10 \\ \dfrac{1}{2} - \dfrac{\ln(2\mu)}{2\mu^2}, & \mu > 10. \end{cases} \tag{18}$$

Finally, for A_{EH}, μ in the Eshelby tensor is that of the CNT, i.e., $\mu = l_{CNT}/\left(2r_{CNT}\right)$. For A_{CN}, μ in the Eshelby tensor is obtained considering the limit as $l_{CNT} \to \infty$ [30,32].

3.2. Two-parameter model for agglomeration and segregation

To include agglomeration, we follow a two-parameter model originally proposed by Shi et al. [41] for the elastic properties of CNT composites. They defined two agglomeration parameters:

$$\chi = \frac{V_b}{V}, \tag{19}$$

$$\zeta = \frac{V_r^b}{V_r}, \tag{20}$$

where V_b is the total volume of the regions that encapsulate CNT agglomerations which we will call "bundles", V is the volume of the nanocomposite, V_r is the total volume of CNTs inside the nanocomposite, and V_r^b is the volume of CNTs inside the bundles. Parameter χ represents the volume fraction of bundles in the nanocomposite, which are indicated with blue circles in the 2D schematic of Fig. 3. On the other hand, parameter ζ represents the fraction of CNTs located inside the bundles.

In the original two-parameter agglomeration model by Shi et al. [41], as well as in other works [42–45], similar descriptions of χ and ζ have been given. It has been stated that whenever $\chi = 1$ or $\chi = \zeta$ results in a homogeneous distribution of the CNTs. However, we observe that $\chi = 1$ resulting in a homogeneous distribution in the composite implies CNTs actually have a homogeneous distribution inside bundles. This is because $\chi = 1$ means all the volume of the nanocomposite consists of bundles. Then, in order to have a homogeneous distribution overall in the composite, the bundles must also have a homogeneous distribution. Also note that $\chi = 1$ requires $\zeta = 1$ as the only possible value as there cannot be CNTs outside the bundles if the whole nanocomposite is made up of bundles. Similarly, when $\chi = \zeta$, the ratio of volume for bundles and nanocomposite volume is the same as the ratio of CNTs inside bundles and outside of them. This results in having the same CNT concentration both inside and outside the bundles. Then, for this to

result in an overall homogeneous distribution of CNTs in the composite, CNTs inside the bundles must have a homogeneous distribution. From our perspective, a homogeneous distribution of CNTs inside bundles does not represent agglomeration accurately.

Another common observation of this two-parameter model is that $\zeta > \chi$ represents an agglomerated state. The larger the value of ζ the more severe the agglomeration [32,41,46]. However, to the knowledge of the authors, the case when $\zeta < \chi$ has not been explored. Here we observe that when $\zeta < \chi$, there are some regions of the matrix (the bundles) that contain low amounts of CNTs. As a consequence, the rest of the matrix contains the majority of CNTs in the composite. The larger the value of χ, the larger the size of the regions with low content of CNTs. This is characteristic of a segregated structure. Then, it is clear that the two parameters for agglomeration, ζ and χ, can also be used to describe segregation when $\zeta < \chi$.

Thus, given the observations presented in the previous paragraphs, here we add a new perspective for the two parameters ζ and χ and present a two-parameter model for agglomeration and segregation. First, we assume the CNTs inside the bundles are entangled and not homogeneously distributed as implied by the original model. Fig. 3 illustrates the new assumption, where CNTs are entangled inside the bundles. This new assumption results in having no electrical percolation inside the bundles. On the other hand, outside the bundles in what we will refer to as the "dispersed matrix", CNTs are assumed to be homogeneously dispersed. It is only in the dispersed matrix that there may be percolation.

It should be noted that the Eshelby–Mori–Tanaka theory is based on the assumption that the inclusions are homogeneous and, therefore, it may not be an ideal choice for modeling composites with non-homogeneous inclusions, as in this study. To overcome this inconsistency, a few studies employed a double-inclusion approach [47,48], to capture mechanical characteristics of composites with non-homogeneous inclusions. In principle, the double-inclusion approach seems more suitable to model nanocomposites comprising bundles (inclusions with an inner inclusion consisting of the entangled CNTs). Such an approach would adequately describe the bundles surrounded by interphases, facilitating modeling of segregated clusters as highly loaded inclusions surrounded by lowly loaded interphases. Nevertheless, due to its simplicity and its robustness in capturing measured electrical response (see Section 4.2) we consider the Eshelby–Mori–Tanaka approach as a first approximation in this study.

Given the new assumptions, the domain for all possible (ζ, χ) pairs is shown in Fig. 4. In principle, both ζ and χ fall in the range $[0, 1]$. However, considering physical constraints these two parameters cannot take all possible values within that range, e.g., $\chi = 1$ requires $\zeta = 1$ as observed earlier. First, the minimum possible value for V_b is V_r^b as the bundles must at least contain the CNTs inside them, i.e., $\chi \geq V_r^b/V$. By substituting Eq. (20) into this expression we obtain the following lower limit for χ:

$$\chi \geq \phi\zeta. \tag{21}$$

Second, the volume of the dispersed matrix is $V - V_b = (1-\chi)V$. This volume must be at least equal to the volume of CNTs in the dispersed matrix, which is given by $V_r - V_r^b$. Thus, $(1-\chi)V \geq V_r - V_r^b$ and by using Eq. (20) we obtain the following upper limit for χ:

$$\chi \leq 1 + \phi(\zeta - 1). \tag{22}$$

The set of (ζ, χ) pairs that fall outside the limits imposed by Eqs. (21) and (22) are indicated in Fig. 4 with dark blue shading. Any (ζ, χ) pair within the shaded areas in dark blue has no physical meaning.

Fig. 4 also shows four limiting cases of the microstructure in the composite. It is observed that the case for homogeneous distribution is reduced to the case when $\zeta = 0$ and $\chi = 0$. We consider that reducing homogeneous distribution to a single point instead of the lines $\zeta = \chi$ and $\chi = 1$ contributes to widening the range of microstructures that may be represented with this two-parameter model. In Fig. 4 a limiting

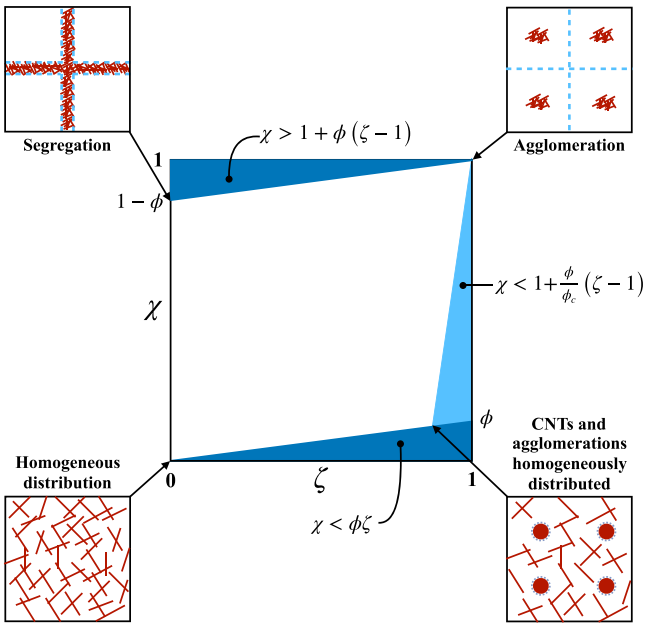

Fig. 4. Domain for agglomeration and segregation parameters ζ and χ. Four limiting cases of the microstructure are observed: homogeneous distribution of CNTs ($\zeta = 0$, $\chi = 0$), segregation ($\zeta = 0$, $\chi = 1 - \phi$), agglomeration ($\zeta = 1$, $\chi = 1$), homogeneous distribution of agglomerations and CNTs. Non-meaningful part of the domain is shaded in dark blue. The part of the domain with no percolation in the dispersed matrix is shaded in light blue.

case of segregation is observed when $\zeta = 0$ and $\chi = 1 - \phi$. In that figure, dashed blue lines represent bundles boundaries. It is observed that pairs such that $\chi > \zeta$ tend to be a segregated structure. A limiting case of agglomeration is observed when $\zeta = 1$ and $\chi = 1$. Here, there are clusters of entangled CNTs homogeneously distributed inside the matrix. There is also an example of a homogeneous distribution of CNTs and agglomerations at the intersection of lines $\chi = \phi\zeta$ and $\chi = 1 + (\phi/\phi_c)(\zeta - 1)$. For that limiting case, the volume of bundles consists only of CNTs without polymer and, thus, agglomerations are represented as filled circles. The limiting factors that result in the line $\chi = 1 + (\phi/\phi_c)(\zeta - 1)$ are explained in the next subsection.

It is observed that in this work we present the first full description of the domain for the agglomeration parameters ζ and χ. Fig. 4 illustrates the wide range of microstructures that can be represented with these two parameters given our newly added perspective, which makes it possible to include agglomeration and segregation.

3.3. Electrical conductivity considering agglomeration and segregation

To calculate the electrical conductivity of CNT-based PNCs using the two-parameter agglomeration and segregation model we follow a two step process:

- Calculate the electrical conductivity inside bundles, σ_{eff}^b, and inside the dispersed matrix, σ_{eff}^d.
- Calculate the electrical conductivity of the composite that consists of a matrix with electrical conductivity σ_{eff}^d containing inclusions with electrical conductivity σ_{eff}^b.

For the first step, the electrical conductivity inside the bundles, σ_{eff}^b, is obtained only considering the contribution from electron hopping. This is because we are now assuming there is no percolation inside the bundles. Thus, the electrical conductivity inside the bundles is calculated as:

$$\sigma_{eff}^b = \sigma_M + \sigma_{EH}^b. \tag{23}$$

However, the CNT content is updated as, instead of ϕ, the volume fraction of CNTs inside the bundles is given by [41]:

$$\phi_b = \frac{\zeta}{\chi}\phi. \tag{24}$$

For the dispersed matrix, since there are contributions from both electron hopping and conductive networks, its conductivity is calculated as:

$$\sigma^d_{eff} = \sigma_M + \left(1 - \eta\left(\phi_d\right)\right)\sigma^d_{EH} + \eta\left(\phi_d\right)\sigma^d_{CN}, \tag{25}$$

where ϕ_d is the CNT content in the dispersed matrix and is calculated as [41]:

$$\phi_d = \frac{1-\zeta}{1-\chi}\phi. \tag{26}$$

For the second step, the conductivity of the composite with agglomeration (or segregation) is obtained by considering the bundles to be ellipsoidal inclusions with conductivity σ^b_{eff} distributed in a matrix with conductivity σ^d_{eff}. Given the new definition of the bundles containing entangled CNTs, the ellipsoidal inclusions do not form a percolated network. Thus, the conductivity of the composite is calculated as:

$$\sigma_{eff} = \sigma^d_{eff} + \sigma_{EH}, \tag{27}$$

where

$$\sigma_{EH} = \frac{\int_0^{2\pi}\int_0^{\pi} p(\varphi,\psi)\left(Q^T\sigma^b_{eff}Q - \sigma^d_{eff}\right)A^b_{EH}\sin(\varphi)\,d\varphi d\psi}{\int_0^{2\pi}\int_0^{\pi} p(\varphi,\psi)\sin(\varphi)\,d\varphi d\psi}. \tag{28}$$

Here, the content of fillers, i.e., bundles, is equal to χ. To calculate the Eshelby tensor as part of obtaining A^b_{EH} in Eq. (28), we use the following expressions for the S_{22} component:

$$S_{22} = \begin{cases} \dfrac{\mu_e}{2\left(1-\mu_e^2\right)^{3/2}}\left[\cos^{-1}\mu_e - \mu_e\left(1-\mu_e^2\right)^{1/2}\right], & \mu_e < 1 \\ \dfrac{\mu_e}{2\left(\mu_e^2-1\right)^{3/2}} \times \left[\mu_e\left(\mu_e^2-1\right)^{1/2} - \ln\left(\mu_e + \left(\mu_e^2-1\right)^{1/2}\right)\right], & 1 < \mu_e \le 10 \\ \dfrac{1}{2} - \dfrac{\ln\left(2\mu_e\right)}{2\mu_e^2}, & 10 < \mu_e. \end{cases} \tag{29}$$

where μ_e is the aspect ratio of the ellipsoidal bundles, where two of their axes are assumed to be equal [30,32]. S_{11} is computed as in Eq. (16).

From Eqs. (24) and (26) it is clear that whenever $\chi = 0$ or $\chi = 1$ results in division by zero. Thus, in our implementation of the model, these cases are treated separately. When $\chi = 0$ (which requires $\zeta = 0$), there are no bundles so the electrical conductivity of the composite is that of the dispersed matrix, i.e., $\sigma_{eff} = \sigma^d_{eff}$. When $\chi = 1$ (which requires $\zeta = 1$), there are only agglomerations and there is no percolation. In this case the conductivity of the composite is that of the bundles, i.e., $\sigma_{eff} = \sigma^b_{eff}$.

Finally, we note that if there is no percolation inside the dispersed matrix, i.e., $\phi_d < \phi_c$, then there is no percolation in the composite. Thus, whenever this happens the electrical conductivity of the composite is only due to electron hopping. In that case, the conductivity of the composite is calculated as $\sigma_{eff} = \sigma_M + \sigma_{EH}$. This will yield the same results independently of the values of ζ and χ. Thus, the case when $\phi_d < \phi_c$ defines a region of equal conductivity and using Eq. (26) we obtain the following limit:

$$\chi < 1 + \frac{\phi}{\phi_c}(\zeta - 1). \tag{30}$$

The region limited by Eq. (30) is indicated in Fig. 4 with light blue shading. It is noted that, while parameters ζ and χ may take values within this region, the electrical conductivity is computed differently as mentioned previously.

4. Results and discussion

4.1. Characterization of CNTs

Surface characteristics of as received CNTs were analyzed based on SEM results, revealing that the CNTs are highly entangled and share common walls, as shown in Fig. 5. The average length of the CNT is > 30 μm and its average outer diameter is 10 nm, with aspect ratio of individual CNT > 3000 [11]. XRD patterns for CNTs shown in Fig. 6a exhibit a peak due to (002) plane at about $2\theta = 26°$ and is derived from the ordered arrangement of the concentric cylinders of graphitic carbon. The peaks around $2\theta = 43°$ are due to the (110) graphitic planes plus small amounts of catalyst particles encapsulated inside the walls of the CNTs. Raman spectra show the characteristic "D" and "G" bands of CNTs (Fig. 6b). The D band is related to the sp^3 state of carbon and can be used as a proof of disruption of the aromatic π-electrons (sp^2 hybridized) of CNTs, i.e., presence of defects. In contrast, the G band is related to the graphitic structure (sp^2 carbons). The intensity of the D band gives information about the amount of amorphous carbon and defects present in the CNT. The defects in the CNTs are related with their crosslinking, wall sharing and branching characteristics. As SEM images confirmed the CNTs are highly entangled. The higher intensity of the D band might be due to the higher entanglement density of CNTs [5]. Fig. 6c shows the thermogravimetric (TG) and derivative thermogravimetric (DTG) traces of CNT. TG/DTG traces were recorded in oxygen atmosphere (flow rate 20 ml/min) for CNT. A heating rate of 20 °C/min and sample size of 10 ± 1 mg were used. Single step degradation was observed for CNTs. The onset temperature of CNT is ~ 555 °C. The total mass loss up to 800 °C was ~ 90 % with CNT due to oxidation or burn out of carbon nanotubes which was used indirectly for the determination of purity of CNT.

Fig. 7 shows the SEM micrographs of CNT/HDPE and CNT/PLA nanocomposites at CNT loadings of 2 and 6 wt. %. The SEM scan suggests a uniform dispersion of CNTs in both matrices. A uniform dispersion of CNTs usually facilitates the formation of a percolated network in polymer matrices. However, assessing the dispersion state of CNTs in PNCs is limited by the area observed in SEM images [17]. Thus, in the scanned areas of the PNC, a uniform dispersion might be observed while in other areas agglomeration or even segregation might take place. This may be the case in our samples as, comparing Fig. 7a with Fig. 7c, it is observed that the CNT content is the same but more CNTs are observed in the HDPE matrix.

4.2. Electrical conductivity of CNT/PLA and CNT/HDPE nanocomposites: measurements and predictions

Figs. 8a and 8b show the measured of DC conductivity of CNT/PLA and CNT/HDPE nanocomposites respectively as a function of CNTs volume fraction (vol. %). In experiments, CNT content is typically measured in weight fraction (see Section 2). However, to be consistent with our model predictions, experimental results are also presented in volume fraction. From the plots it is clear that the conductivity of the nanocomposites increases with CNT loading, as expected, and displays a sharp rise with initial loading of CNTs. The sudden change in the conductivity values suggests the onset of percolation. In the present study, the percolation threshold has been calculated by plotting the electrical conductivity as a function of the percentage volume fraction of CNTs and performing data fitting with a power law function from percolation theory [5,49,50]:

$$\sigma = \sigma_0\left(\phi - \phi_c\right)^{\beta}; \quad \phi > \phi_c. \tag{31}$$

where σ and σ_0 are the electrical conductivity of conductive polymer nanocomposite and intrinsic conductivity constant, respectively, and β is the critical exponent which is related to the dimensionality of the conductive network [14]. The linear regression data fitting results in $\phi_c = 0.23$ vol. % and $\beta = 3.98$ for CNT/PLA composites and $\phi_c =$

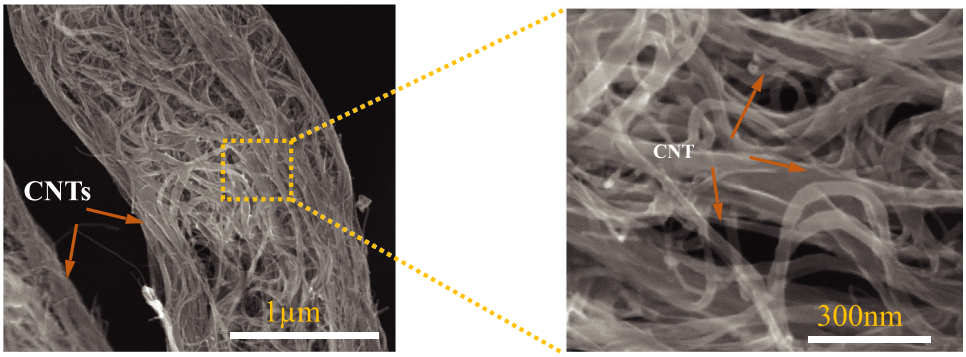

Fig. 5. SEM micrograph of neat as received CNTs showing wall sharing. Image on the right is a magnification of the squared region indicated in the image on the left.

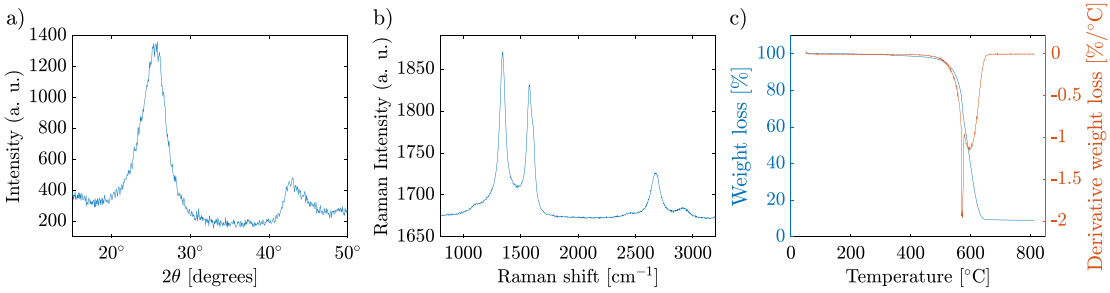

Fig. 6. Characterization of CNTs. (a) XRD spectrum of CNT (b) Raman plot of CNT, and (c) TG/DTG traces of CNT in air atmosphere with heating rate 20 °C/min.

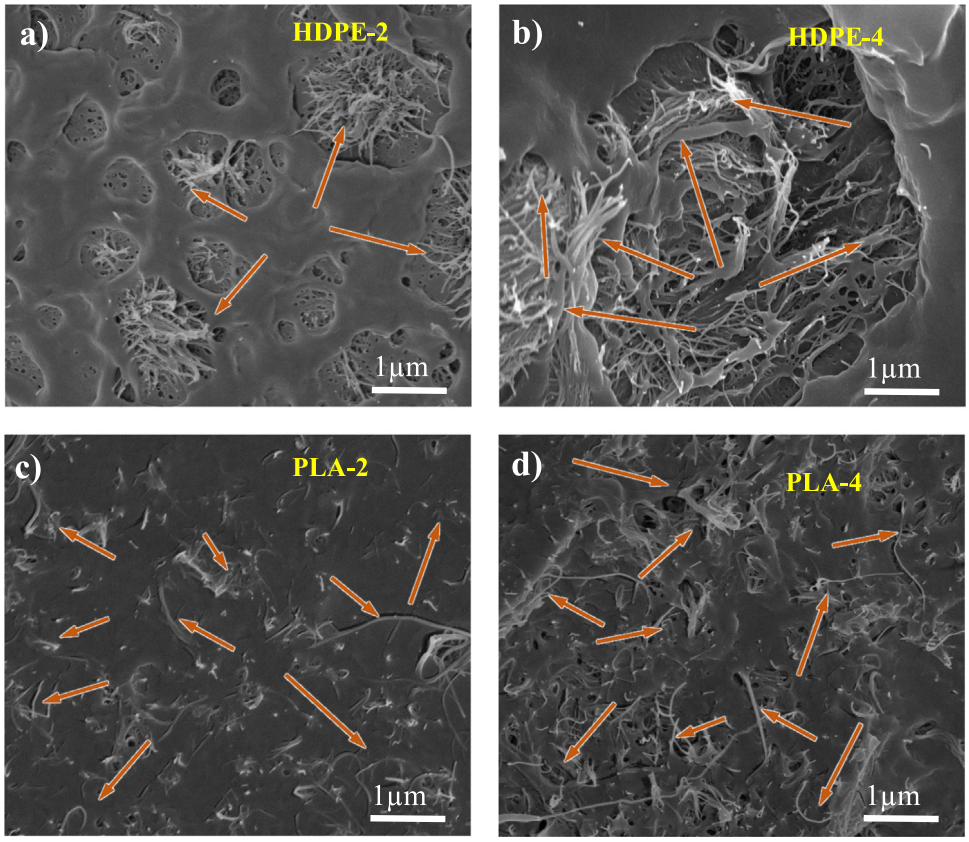

Fig. 7. SEM micrograph of CNT/HDPE nanocomposites at (a) 2 wt. % and (b) 4 wt. % and CNT/PLA nanocomposites at (c) 2 wt. % and (d) 4 wt. %. Arrows indicate the presence of CNTs.

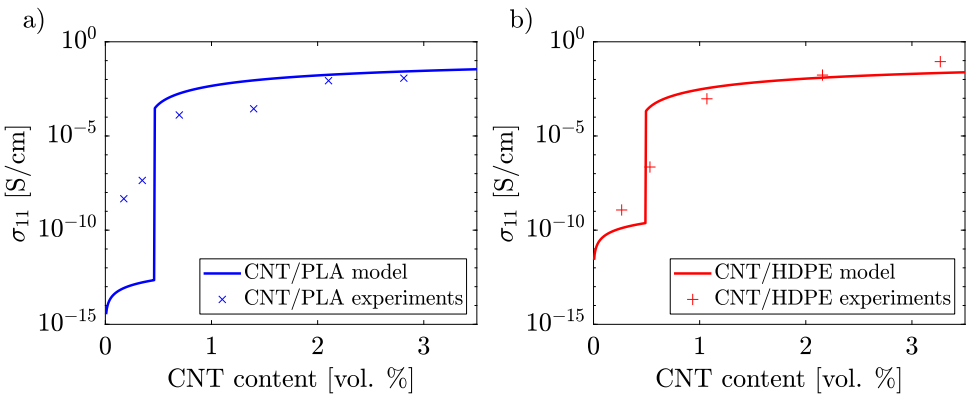

Fig. 8. Electrical conductivity of 3D printed (a) PLA/CNT and (b) HDPE/CNT nanocomposites. Experimental results are shown with symbols while simulation results are shown in solid lines.

Table 1
Parameters found to reproduce experimental data using our electrical conductivity model for segregation and agglomeration. The '(s)' in the last two rows indicates that the composites were fabricated with CNT segregation.

Polymer	ϕ_c^h [vol. %]	χ	ζ
PLA	0.3239	0.4502	0.6132
HDPE	0.2417	0.4463	0.7281
UHMWPE	0.0174	0.4482	0.4378
PDMS	0.0148	0.4487	0.4128
TPU	0.0723	0.4431	0.5373
HDPE (s)	0.0099	0.9024	0.6959
TPU (s)	0.0050	0.4309	0.1707

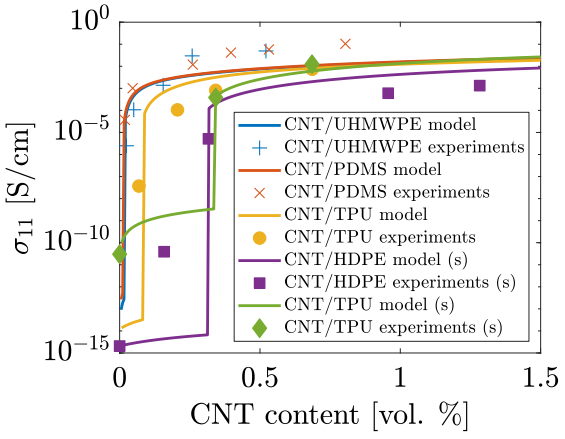

Fig. 9. Comparison of predicted values with measured values of electrical conductivity of polymer nanocomposites reported in the literature: CNT/UHMWPE [55], CNT/PDMS [11], CNT/TPU [8], CNT/HDPE with segregation (s) [57], and CNT/TPU with segregation (s) [56].

0.18 vol. % and $\beta = 5.31$ for CNT/HDPE composites. The lower ϕ_c for HDPE can be primarily attributed to its semi-crystalline nature. CNTs have been found to disperse in the amorphous phase of a polymer as they are ejected form the crystalline phase [51,52]. Thus, CNTs tend to concentrate in the amorphous phase, which is a fraction of the volume of the whole matrix. Then it is easier for CNTs to form a percolated network.

In Fig. 8 we present simulation results from our agglomeration and segregation model for CNT/PLA and CNT/HDPE nanocomposites as solid lines. We observe from Fig. 8 that our model reproduces the measurements well. We use commonly reported values for CNT composites for $d_c = 1.8$ nm [26,37] and $\lambda = 1.5$ eV [16,32], while we took $\sigma_M = 10^{-16}$ S/cm for PLA [53,54]. We used Matlab's optimization function `fmincon` to find the CNT conductivity, percolation threshold, and parameters χ and ζ that best fit the measured data. We found one CNT conductivity for all CNT/polymer composites and a percolation threshold, χ and ζ for each CNT/polymer composite. The percolation threshold is considered to be a fitting parameter as the one calculated from measured data using Eq. (31) includes the effects of the agglomerated or segregated state of the composite. However, as the electrical conductivity model assumes homogeneous distribution of CNTs, then we also require the percolation threshold for a homogeneous distribution of CNTs. Thus, we also find the percolation threshold for homogeneous distribution, ϕ_c^h. We found $\sigma_{CNT} = 9.87$ S/cm while the rest of fitting parameters are presented in Table 1. From this table we observe that χ is very similar for both CNT/PLA and CNT/HDPE nanocomposites. Also, χ and ζ do not differ much for both cases which means there is a homogeneous distribution of CNTs with some agglomerations. Also, dispersion quality is similar as bundles tend to occupy the same volume and have similar content of CNTs.

We also compared results from our electrical conductivity model with data reported in the literature for CNT-based PNCs with different matrices: ultra-high-molecular-weight-polyethylene (UHMWPE) [55], polydimethylsiloxane (PDMS) [11], thermoplastic polyurethane (TPU) [8,56], and HDPE [57]. In the aforementioned studies, Yuan et al. [56] and Du et al. [57] fabricated CNT/polymer composites with CNT segregation. Thus, by comparing results from our model with measurements of samples with CNT segregation, we can assess the capabilities of our model. Results shown in Fig. 9, indicate a good agreement between measurements and predictions. To assess the goodness of the fit, we calculated the root-mean-square deviation as 0.0228 which indeed indicates a good fit. Fitting parameters are also shown in Table 1. In both Fig. 9 and Table 1 an '(s)' indicates the composites that were fabricated with CNT segregation. From the last two rows of Table 1, it is observed that $\chi > \zeta$ for the composites fabricated with segregation. Moreover, the differences in the values of the parameters indicate a large degree of segregation, compared to the rest of parameters shown in Table 1. This confirms that our model can accurately capture CNT segregation observed in experimental samples. For the rest of composites taken from the literature, χ is similar for all cases. We also observe that CNT/UHMWPE and CNT/PDMS are slightly segregated as $\chi > \zeta$. However, as the difference between χ and ζ is small, there will be homogeneously distributed CNTs with some agglomerations as in the rest of the CNT/polymer composites. In addition, we note that our model is able to capture the electro-conductive behavior of both thermoplastic (HDPE, PLA, UHMWPE) and elastomeric (PDMS, TPU) polymer nanocomposites loaded with CNTs. This shows the versatility of our model in capturing the macroscopic electrical conductivity of different PNCs.

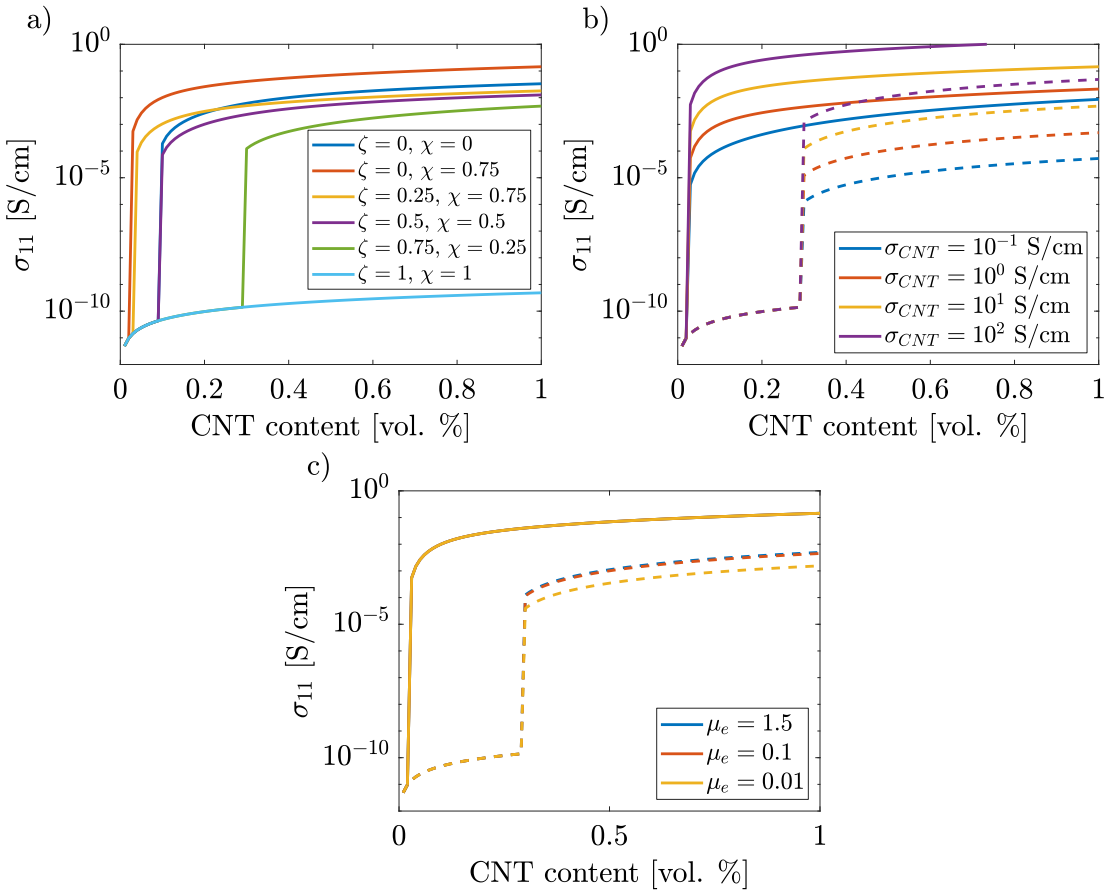

Fig. 10. Sensitivity analysis of our electrical conductivity model for agglomeration and segregation. (a) Effect of parameters ζ and χ. (b) Effect of CNT conductivity, σ_{CNT}. (c) Effect of aspect ratio of bundles, μ_e. In (b) and (c) solid lines correspond to a segregated state ($\zeta = 0$, $\chi = 0.75$) and dashed lines correspond to an agglomerated state ($\zeta = 0.75$, $\chi = 0.25$). Other parameters used are $\lambda = 0.5$ eV, $\sigma_{CNT} = 10$ S/cm, $\sigma_M = 10^{-13}$ S/cm, and $\mu_e = 5$, unless otherwise stated.

4.3. Sensitivity analysis of agglomeration/segregation model

In this section, we perform a sensitivity analysis to study the response of our electrical conductivity model to changes in certain parameters. The chosen parameters for the sensitivity analysis are ζ, χ, CNT conductivity (σ_{CNT}) and bundle aspect ratio (μ_e). Results of the sensitivity analysis are presented in Fig. 10, where we show the component σ_{11} of the effective electrical conductivity ($\sigma^L_{CNT} = \sigma^T_{CNT} = \sigma_{CNT}$). We use the same values for d_c and λ as in Section 4.2. We use the electrical conductivity of an HDPE matrix, i.e., $\sigma_M = 10^{-13}$ S/cm [58]. CNT geometries used are the same as that of CNTs reported in Section 2.

In Fig. 10a, we present the effective electrical conductivity for different values of (ζ, χ) pairs. For the curve where $\zeta > \chi$, electrical conductivity is lower and percolation threshold is larger than that for homogeneous distribution (i.e., when $\zeta = \chi = 0$). This implies the presence of CNT agglomerates as they reduce the probability of forming a percolated network [2]. However, it has been reported that agglomeration may result in increased electrical conductivity [17,59,60]. In such cases it is likely that the agglomerations actually form a segregated structure (e.g., compare Figure 2 in [59] with Figure 2a in [15]). For the curves in Fig. 10a where $\zeta < \chi$, electrical conductivity is always higher compared to the curve for homogeneous distribution. It is also observed that percolation starts at lower volume fractions. This implies segregation since CNTs are closer to each other inside a smaller volume (i.e., the dispersed matrix), which results in effectively increasing the CNT content in the dispersed matrix above the percolation threshold of homogeneously dispersed CNTs. This result can also be observed from Eq. (26), where clearly $\phi_d > \phi$ when $\zeta < \chi$. This result also implies that the effective percolation threshold of the composite is reduced.

In Fig. 10b, we present the effect of CNT conductivity, σ_{CNT}, on the conductivity of composites. In Fig. 10b, solid lines correspond to a segregated state ($\zeta = 0$, $\chi = 0.75$) while dashed lines correspond to an state with CNT agglomerates ($\zeta = 0.75$, $\chi = 0.25$). In both segregated and agglomerated states increasing or decreasing the CNT conductivity results in an increase or decrease in the effective electrical conductivity, respectively. The main effect of varying σ_{CNT} is to move the electrical conductivity curve up or down as σ_{CNT} increases or decreases, respectively. This is expected as the main contribution towards the composite's conductivity comes from the CNTs.

In Fig. 10c, we present the effect of bundle aspect ratio, μ_e. Again we present results for segregated ($\zeta = 0$, $\chi = 0.75$) and agglomerated states ($\zeta = 0.75$, $\chi = 0.25$) with solid and dashed lines, respectively. We observe that the bundle aspect ratio has no effect on the conductivity of the composite with segregation. In contrast, we observe that as the aspect ratio of bundles is decreased, the conductivity of composites with agglomeration also decreases. We also observe that for $\mu_e > 1$ there is no noticeable change in conductivity for segregated and agglomerated composites. We note that García-Macías et al. [32] observed changes in electrical conductivity for $\mu_e > 1$. However, this is likely to happen due to two differences with the composites they studied. First, the differences in conductivity between matrix and nanofillers are far larger in our study. Second, we assume no percolation in the bundles while García-Macías et al. [32] use definitions of ζ and χ that imply homogeneous distribution of CNTs in bundles (see Section 3.2) allowing them to percolate. Thus, in our model, the contribution of bundles is far lower, which explains their limited effect on the conductivity of the nanocomposite.

5. Conclusions

We in-house nanoengineered filament feedstocks and successfully fabricated electrically conductive PLA/CNT and HDPE/CNT composites via FFF additive manufacturing. Electrical conductivity of 3D printed PNCs was measured. We developed a micromechanics-based model for predicting electrical conductivity of PNCs that exhibit agglomeration and segregation of CNTs. By adding a new perspective to a two-parameter agglomeration model, we demonstrated that the model can capture the effect of CNT segregation on electrical conductivity. We presented a full description of the two agglomeration parameters and showed a wide range of microstructures that can be captured with this model. Furthermore, a good agreement between electrical conductivity measurements and predictions, demonstrates the robustness of our agglomeration and segregation model. These results also highlight the capabilities of our model in obtaining information regarding PNC's microstructure, e.g., whether there is agglomerated or segregated CNT dispersion. We further validated our model with conductivity measurements reported in the literature, demonstrating its utility in capturing the electro-conductive characteristics of both thermoplastic and elastomeric PNCs.

Declaration of competing interest

The authors declare that they have no known competing financial interests or personal relationships that could have appeared to influence the work reported in this paper.

Acknowledgment

We gratefully acknowledge financial support from the Abu Dhabi National Oil Company (ADNOC), United Arab Emirates under Award No: EX2016-000010.

Appendix A. Supplementary data

Supplementary material related to this article can be found online at https://doi.org/10.1016/j.compositesb.2019.107600.

References

[1] Iijima S. Helical microtubules of graphitic carbon. Lett Nature 1991;354(6348):56–8.
[2] Wernik JM, Meguid SA. Recent developments in multifunctional nanocomposites using carbon nanotubes. Appl Mech Rev 2010;63(5):050801.
[3] Baughman RH, Zakhidov AA, de Heer WA. Carbon nanotubes–the route toward applications. Science 2002;297(5582):787–92.
[4] Moniruzzaman M, Winey KI. Polymer nanocomposites containing carbon nanotubes. Macromolecules 2006;39(16):5194–205.
[5] Verma P, Saini P, Malik RS, Choudhary V. Excellent electromagnetic interference shielding and mechanical properties of high loading carbon-nanotubes/polymer composites designed using melt recirculation equipped twin-screw extruder. Carbon 2015;89:308–17.
[6] Verma P, Saini P, Choudhary V. Designing of carbon nanotube/polymer composites using melt recirculation approach: Effect of aspect ratio on mechanical, electrical and EMI shielding response. Mater Des 2015;88:269–77.
[7] Kennel EB. Electrical properties of nanoparticle-filled polymers. In: Polymer nanocomposites handbook. CRC Press; 2009 [chapter 16].
[8] Kumar S, Gupta TK, Varadarajan K. Mechanically strong, stretchable and ultrasensitive MWCNT/TPU nanocomposites. Composites B 2019.
[9] Ramalingame R, Hu Z, Gerlach C, Kanoun O. Shoe insole with MWCNT-PDMS-composite sensors for pressure monitoring. Proc IEEE Sensors 2017;1–3.
[10] Ku-Herrera JJ, La Saponara V, Avilés F. Selective damage sensing in multiscale hierarchical composites by tailoring the location of carbon nanotubes. J Intell Mater Syst Struct 2018;29(4):553–62.
[11] Arif MF, Kumar S, Gupta TK, Varadarajan KM. Strong linear-piezoresistive-response of carbon nanostructures reinforced hyperelastic polymer nanocomposites. Composites A 2018;113:141–9.
[12] Sanli A, Benchirouf A, Müller C, Kanoun O. Piezoresistive performance characterization of strain sensitive multi-walled carbon nanotube-epoxy nanocomposites. Sensors Actuators A 2017;254:61–8.
[13] Zhang W, Dehghani-Sanij AA, Blackburn RS. Carbon based conductive polymer composites. J Mater Sci 2007;42(10):3408–18.
[14] Stauffer D, Aharony A. Introduction to percolation theory. 2nd ed. Taylor & Francis; 1994.
[15] Pang H, Xu L, Yan DX, Li ZM. Conductive polymer composites with segregated structures. Prog Polym Sci 2014;39(11):1908–33.
[16] Hu B, Hu N, Li Y, Akagi K, Yuan W, Watanabe T, et al. Multi-scale numerical simulations on piezoresistivity of CNT/polymer nanocomposites. Nanoscale Res Lett 2012;7:402.
[17] Mutiso RM, Winey KI. Electrical properties of polymer nanocomposites containing rod-like nanofillers. Prog Polym Sci 2015;40:63–84.
[18] Nadgorny M, Ameli A. Functional polymers and nanocomposites for 3D printing of smart structures and devices. ACS Appl Mater Interfaces 2018;10(21):17489–507.
[19] Kumar S, Wardle BL, Arif MF. Strength and performance enhancement of bonded joints by spatial tailoring of adhesive compliance via 3D printing. ACS Appl Mater Interfaces 2017;9(1):884–91.
[20] Arif MF, Kumar S, Varadarajan KM, Cantwell WJ. Performance of biocompatible PEEK processed by fused deposition additive manufacturing. Mater Des 2018;146:249–59.
[21] Gnanasekaran K, Heijmans T, van Bennekom S, Woldhuis H, Wijnia S, de With G, et al. 3D printing of CNT- and graphene-based conductive polymer nanocomposites by fused deposition modeling. Appl Mater Today 2017;9:21–8.
[22] Wang X, Jiang M, Zhou Z, Gou J, Hui D. 3D printing of polymer matrix composites: A review and prospective. Composites B 2017;110:442–58.
[23] Liljenhjerte J, Upadhyaya P, Kumar S. Hyperelastic strain measurements and constitutive parameters identification of 3D printed soft polymers by image processing. Addit Manuf 2016;11:40–8.
[24] Kumar S, Wardle BL, Arif MF, Ubaid J. Stress reduction of 3D printed compliance-tailored multilayers. Adv Energy Mater 2018;20(1):1–8.
[25] Khan MA, Kumar S. Performance enhancement of tubular multilayers via compliance-tailoring: 3D printing, testing and modeling. Int J Mech Sci 2018;140(February):93–108.
[26] Mora A, Han F, Lubineau G. Estimating and understanding the efficiency of nanoparticles in enhancing the conductivity of carbon nanotube/polymer composites. Results Phys 2018;10:81–90.
[27] Li C, Thostenson ET, Chou T-W. Effect of nanotube waviness on the electrical conductivity of carbon nanotube-based composites. Compos Sci Technol 2008;68(6):1445–52.
[28] Seidel G, Lagoudas D. A micromechanics model for the electrical conductivity of nanotube-polymer nanocomposites. J Compos Mater 2009;43(9):917–41.
[29] Pal G, Kumar S. Multiscale modeling of effective electrical conductivity of short carbon fiber-carbon nanotube-polymer matrix hybrid composites. Mater Des 2016;89:129–36.
[30] Feng C, Jiang L. Micromechanics modeling of the electrical conductivity of carbon nanotube (CNT)-polymer nanocomposites. Composites A 2013;47:143–9.
[31] Hu N, Karube Y, Yan C, Masuda Z, Fukunaga H. Tunneling effect in a polymer/carbon nanotube nanocomposite strain sensor. Acta Mater 2008;56(13):2929–36.
[32] García-Macías E, D'Alessandro A, Castro-Triguero R, Pérez-Mira D, Ubertini F. Micromechanics modeling of the electrical conductivity of carbon nanotube cement-matrix composites. Composites B 2017;108:451–69.
[33] Gong S, Zhu Z, Meguid S. Carbon nanotube agglomeration effect on piezoresistivity of polymer nanocomposites. Polymer 2014;55(21):5488–99.
[34] Mora A, Han F, Lubineau G. Computational modeling of electrically conductive networks formed by graphene nanoplatelet-carbon nanotube hybrid particles. Modelling Simulation Mater Sci Eng 2018;26(3):035010.
[35] Park SH, Hwang J, Park GS, Ha JH, Zhang M, Kim D, et al. Modeling the electrical resistivity of polymer composites with segregated structures. Nature Commun 2019;10(1).
[36] Zhao H, Bai J. Highly sensitive piezo-resistive graphite nanoplatelet-carbon nanotube hybrids/polydimethylsilicone composites with improved conductive network construction. ACS Appl Mater Interfaces 2015;7(18):9652–9.
[37] Li C, Thostenson ET, Chou T-W. Dominant role of tunneling resistance in the electrical conductivity of carbon nanotube-based composites. Appl Phys Lett 2007;91(22):223114.
[38] De Vivo B, Lamberti P, Spinelli G, Tucci V. Numerical investigation on the influence factors of the electrical properties of carbon nanotubes-filled composites. J Appl Phys 2013;113(24):244301.
[39] Simmons JG. Generalized formula for the electric tunnel effect between similar electrodes separated by a thin insulating film. J Appl Phys 1963;34(1963):1793–803.
[40] Bauhofer W, Kovacs JZ. A review and analysis of electrical percolation in carbon nanotube polymer composites. Compos Sci Technol 2009;69(10):1486–98.
[41] Shi D-L, Feng X-Q, Huang YY, Hwang K-C, Gao H. The effect of nanotube waviness and agglomeration on the elastic property of carbon nanotube-reinforced composites. J Eng Mater Technol 2004;126(3):250.
[42] García-Macías E, D'Alessandro A, Castro-Triguero R, Pérez-Mira D, Ubertini F. Micromechanics modeling of the uniaxial strain-sensing property of carbon nanotube cement-matrix composites for SHM applications. Compos Struct 2017;163:195–215.

[43] Krishnaswamy JA, Buroni FC, Garcia-Sanchez F, Melnik R, Rodriguez-Tembleque L, Saez A. Lead-free piezocomposites with CNT-modified matrices: Accounting for agglomerations and molecular defects. Compos Struct 2019;224:111033.
[44] Pan J, Bian L. A physics investigation for influence of carbon nanotube agglomeration on thermal properties of composites. Mater Chem Phys 2019;236(March):121777.
[45] Ji XY, Cao YP, Feng XQ. Micromechanics prediction of the effective elastic moduli of graphene sheet-reinforced polymer nanocomposites. Modelling Simulation Mater Sci Eng 2010;18(4).
[46] Sobhaniaragh B, Batra RC, Mansur WJ, Peters FC. Thermal response of ceramic matrix nanocomposite cylindrical shells using Eshelby-Mori-Tanaka homogenization scheme. Composites B 2017;118:41–53.
[47] Hori M, Nemat-Nasser S. Double-inclusion model and overall moduli of multi-phase composites. Trans ASME J Eng Mater Technol 1994;116(3):305–9.
[48] Hu GK, Weng GJ. Connections between the double-inclusion model and the Ponte Castaneda-Willis, Mori-Tanaka, and Kuster-Toksoz models. Mech Mater 2000;32(8):495–503.
[49] Thostenson ET, Li C, Chou TW. Nanocomposites in context. Compos Sci Technol 2005;65(3–4):491–516.
[50] Gupta TK, Choosri M, Varadarajan K, Kumar S. Self-sensing and mechanical performance of CNT/GNP/UHMWPE biocompatible nanocomposites. J Mater Sci 2018;53(11):7939–52.
[51] Al-Saleh MH, Sundararaj U. A review of vapor grown carbon nanofiber/polymer conductive composites. Carbon 2009;47(1):2–22.
[52] Ganß M, Satapathy BK, Thunga M, Weidisch R, Pötschke P, Jehnichen D. Structural interpretations of deformation and fracture behavior of polypropylene/multi-walled carbon nanotube composites. Acta Mater 2008;56(10):2247–61.
[53] Kuan CF, Kuan HC, Ma CCM, Chen CH. Mechanical and electrical properties of multi-wall carbon nanotube/poly(lactic acid) composites. J Phys Chem Solids 2008;69(5–6):1395–8.
[54] Shao S, Zhou S, Li L, Li J, Luo C, Wang J, Li X, Weng J. Osteoblast function on electrically conductive electrospun PLA/MWCNTs nanofibers. Biomaterials 2011;32(11):2821–33.
[55] Reddy SK, Kumar S, Varadarajan KM, Marpu PR, Gupta TK, Choosri M. Strain and damage-sensing performance of biocompatible smart CNT/UHMWPE nanocomposites. Mater Sci Eng C 2018;92:957–68.
[56] Yuan S, Zheng Y, Chua CK, Yan Q, Zhou K. Electrical and thermal conductivities of MWCNT/polymer composites fabricated by selective laser sintering. Composites A 2018;105:203–13.
[57] Du J, Zhao L, Zeng Y, Zhang L, Li F, Liu P, et al. Comparison of electrical properties between multi-walled carbon nanotube and graphene nanosheet/high density polyethylene composites with a segregated network structure. Carbon 2011;49(4):1094–100.
[58] Wypych G. HDPE High density polyethylene. In: Handbook of polymers. 2016, p. 156–63.
[59] Aguilar JO, Bautista-Quijano JR, Avilés F. Influence of carbon nanotube clustering on the electrical conductivity of polymer composite films. Express Polymer Lett 2010;4(5):292–9.
[60] Li C, Thostenson ET, Chou T-W. Sensors and actuators based on carbon nanotubes and their composites: a review. Compos Sci Technol 2008;68(6):1227–49.